Magnetostriction of $AlFe_2B_2$ in high magnetic fields

S. Sharma,[1,*] A. E. Kovalev,[1] D. J. Rebar,[1] D. Mann,[2] V. Yannello,[3] M. Shatruk,[2] A. V. Suslov,[1] J. H. Smith,[1] and T. Siegrist[1,4,*]

[1]*National High Magnetic Field Laboratory, Tallahassee, Florida 32310, USA*

[2]*Department of Chemistry and Biochemistry, Florida State University, Tallahassee, Florida 32306, USA*

[3]*Department of Chemistry, Biochemistry and Physics, University of Tampa, Tampa, Florida 33606, USA*

[4]*Department of Chemical and Biomedical Engineering, FAMU-FSU College of Engineering, Tallahassee, Florida 32310, USA*

(Received 30 July 2020; accepted 25 May 2021; published 17 June 2021)

Using the experimental capability of the x-ray diffraction instrument available at the 25-T Florida split coil magnet at the NHMFL, we investigated the magnetostriction of polycrystalline $AlFe_2B_2$. The magnetostriction was measured in the vicinity of the ferromagnetic transition with $T_C = 280$ K, at 250, 290, and 300 K. $AlFe_2B_2$ exhibits an anisotropic change in lattice parameters as a function of magnetic field near the Curie temperature, and a monotonic variation as a function of applied field has been observed, i.e., the c axis increases significantly while the a and b axes decrease with increasing field in the vicinity of T_C, irrespective of the measurement temperature. The volume magnetostriction decreases with decreasing temperature and changes its sign across T_C. Density functional theory calculations for the nonpolarized and spin-polarized (ferromagnetic) models confirm that the observed changes in lattice parameters due to spin polarization are consistent with the experiment. The relationships for magnetostriction are estimated based on a simplified Landau model that agrees well with the experimental results.

DOI: 10.1103/PhysRevMaterials.5.064409

I. INTRODUCTION

Magnetostriction or magnetoelastic coupling is a strong coupling between magnetic and structural responses, for example, in magnetoelectric multiferroics (type II) [1,2]. It is the common driving mechanism responsible for the use of a material in magnetomechanical devices [3,4] and for magnetic cooling/refrigeration [5,6]. The materials exhibiting magnetostructural coupling demonstrate a range of interesting behaviors, including magnetic shape memory effects [7], magnetocaloric effects [8,9], magnetostriction or magnetic field induced strain [10–12], and very large magnetoresistance [13]. Recently, $AlFe_2B_2$ has gathered considerable attention due to its promising magnetocaloric properties near room temperature [14–17]. Although the change in entropy with magnetic field (H) in this intermetallic compound is moderate when compared to state-of-the-art magnetocaloric materials, such as Gd_5Si_4 and related systems [8,9,18–21], the inexpensive earth-abundant elements and straightforward synthesis make $AlFe_2B_2$ a promising candidate for magnetocaloric applications. The typical value of the isothermal entropy change is 4.1 J/(kg K) at 2 T and 7.7 J/(kg K) at 5 T [14]. The crystal structure of $AlFe_2B_2$ was reported by Jeitschko [22], and the ferromagnetic (FM) transition temperature (T_C) was found to vary between 274 and 320 K depending on the synthesis conditions [14,16,23–28] due to a narrow stoichiometry range, $Al_{1-y}Fe_{1+y}B_2$ ($-0.01 \leqslant y \leqslant 0.01$), with higher T_C values observed for smaller Al/Fe ratios [15]. Neutron diffraction studies showed that the magnetic moments are aligned along the a axis in the FM state [29], while density functional theory (DFT) predicted the moments to be in the ab plane [30].

Recently, Ke *et al.* [30] have studied the electronic structure and magnetic response of AlT_2B_2 (T = Fe, Mn, Cr, Co, Ni) using DFT and suggested that the magnetization is strongly affected by a change in the lattice parameter c, which is perpendicular to the zigzag chains of boron (B) atoms and lies in plane with the [T_2B_2] layers that are parallel to the ac plane (Fig. 1). Consistent with theoretical predictions, Lejeune *et al.* [31] have confirmed that it is indeed the change in the c-axis length and associated $(\text{Fe-Fe})_{x\text{-axis}}$ interatomic distance that has the largest effect on T_C, while T_C depends only weakly on the (b/a) ratio, indicating the negligible role of the a or b axis in affecting T_C. The recent detailed study of magnetic properties of single-crystal $AlFe_2B_2$ suggested itinerant magnetic behavior, based on the Rhodes-Wohlfarth ratio of ∼1.14 [23]. The effect of alloying Mn, Cr, Co, or Ni on the Fe site and C substitution on the B site has also been investigated [30,31], and the effects of pressure have demonstrated that T_C is suppressed by ∼19 K at a pressure of 2.24 GPa [23]. The magnetocrystalline anisotropy field was reported to be 1 T along the b axis and 5 T along the c axis, consistent with the DFT results [30]. Temperature dependent x-ray diffraction (XRD) results on $AlFe_2B_2$ show that both the a and b axes decrease while the c axis increases when cooling the sample from 298 to 200 K [32].

Despite several reports suggesting a strong correlation between magnetic and structural properties [25,30–32], the crystal structure changes of $AlFe_2B_2$ imposed by an external magnetic field have not been reported. A possible reason for this gap is the lack of nontrivial experimental setups where both temperature and magnetic field can be varied in a broad

*Corresponding authors: sharma@magnet.fsu.edu; siegrist@eng.famu.fsu.edu

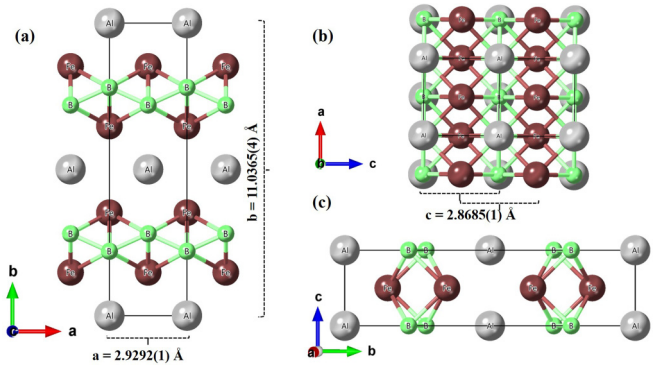

FIG. 1. Unit cell representation of $AlFe_2B_2$ crystal structure in (a) *ab*, (b) *ac*, and (c) *bc* planes. The unit cell parameters indicated in the drawing were obtained by fitting an XRD pattern collected at 300 K and zero applied magnetic field. (Silver spheres: aluminum atoms; green spheres: boron atoms; brown spheres: iron atoms).

range to investigate the evolution of structural properties across the magnetic phase transition as a function of temperature and magnetic field. Furthermore, magnetostriction may lead to material fatigue upon cycling in a magnetocaloric device. Here, we report our experimental study of induced magnetostriction behavior in $AlFe_2B_2$ above and below the FM ordering temperature T_C in magnetic fields up to 25 T. Our results provide direct insight into the structural changes of $AlFe_2B_2$ across T_C and highlight the experimental capabilities of the high magnetic field XRD setup used for the present work. The observed magnetoelastic coupling is analyzed using Landau theory and spin-polarized DFT calculations.

II. EXPERIMENTAL DETAILS

The sample of $AlFe_2B_2$ has been synthesized using arc melting, with the detailed procedure described previously [14]. Briefly, a mixture of starting materials in the Al:Fe:B = 3:2:2 ratio, with a total mass of 0.35 g, was pressed into a pellet, arc-melted, and subjected to annealing at 900 °C for 1 week. The $Al_{13}Fe_4$ byproduct was removed by washing the sample in dilute hydrochloric acid (1:1 *v*/*v*). The sample purity was checked by powder XRD which confirms the single phase nature of the sample [14].

To investigate the magnetoelastic effect in $AlFe_2B_2$, we used a custom diffraction setup integrated with the Florida split coil magnet at the National High Magnetic Field Laboratory (NHMFL) and capable of diffraction in the presence of high DC magnetic field of up to ±25 T [33]. To access the sample space, the magnet has four optical ports defining an angular diffraction range of 45 ° in the forward direction. Higher diffraction angles are available through side ports as described previously [33]. The Mo $K\alpha$ radiation is generated by a Rigaku^{TM} rotating anode source with a maximum power of 18 kW, either Zr-filtered (10 μm) or reflected off a custom multilayer mirror to provide a monochromatized Mo $K\alpha$ radiation spectrum [34]. A Dectris Pilatus 300K-W X^{TM} hybrid pixel detector, customized to tolerate the magnetic fringe fields of the split coil magnet, is used to detect the x-rays at a distance of approximately 1200 mm from the sample. The detector was mounted on a linear slide on an optical table near the x-ray beam exit window to access a wider range of diffraction angles [33]. To analyze the detector images, the DAWN software [35] has been employed to convert the detector images to intensity-vs-2θ data based on geometrical calibration parameters obtained using a NIST SRM 660b LaB_6 reference sample [36]. JANA2006 [37] has been used to Le Bail fit [38] the diffraction data to obtain the field and temperature dependencies of the unit cell parameters. Since the measurements presented here on $AlFe_2B_2$ involve a high DC magnetic field ($\mu_0 H$) of 25 T, the instrument was also calibrated with LaB_6 under the same diffraction condition, temperature, and magnetic field, in order to avoid influencing the data analysis by any effect of magnetic fields on the mechanical setup [33,39]. The results on the LaB_6 sample are given in the Supplemental Material (Fig. S1), together with additional details of the diffraction system [39]. DC magnetization measurements have been performed as a function of temperature and magnetic field to produce an Arrott plot to determine the T_C for the studied sample using a superconducting quantum interference device magnetometer [39].

DFT calculations were accomplished using the Vienna Ab-Initio Simulation Package (VASP) [40]. Published structural parameters of $AlFe_2B_2$ [22] were used for the initial structural geometry, which was subsequently optimized with and without inclusion of spin polarization. PAW-PBE pseudopotentials were used for all elements.

III. RESULTS AND DISCUSSION

Figure 1 shows a representation of the unit cell containing two $AlFe_2B_2$ formula units. Layers of Al atoms alternate with the Fe_2B_2 layers along the *b* axis. The B atoms form zigzag chains that run along the *a* axis while the Fe atoms connect these chains in the *ac* plane [Fig. 1(c)]. The *bc* plane also reveals linear chains of Fe atoms along the *c* axis. The nearest Fe-Fe distance is equal to the *c* lattice parameter.

Figures 2(a) and 2(b) represent the DC magnetization behavior of $AlFe_2B_2$ measured as a function of temperature and magnetic field to determine the onset of ferromagnetic order and to estimate the saturation magnetization of the sample. The magnetization increases sharply when the sample is cooled below 300 K as shown in Fig. 2(a). The inset in Fig. 2(a) shows the isothermal magnetization curve (*M*-vs-*H*) measured at 1.8 K. To determine T_C, Arrott plots are measured at different temperatures and presented in Fig. 2(b) which give $T_C \sim 283$ K, consistent with the literature [14–16,25], and a saturation moment of 2.5 μ_B/f.u.

To determine the magnetostrictive or magnetoelastic interactions derived from the FM exchange coupling between Fe moments, we carried out XRD measurements as a function of applied magnetic field at temperatures of 300, 290, and 250 K. A thin layer of a powdered sample was placed on a copper flat plate sample holder oriented parallel to the magnetic field. The XRD patterns at 300 K were recorded in magnetic fields of 0, 25, and −25 T. At 290 and 250 K, data were collected at 0, 4, 7, 10, 15, 20, and 25 T, and at 250 K, reversed magnetic fields (up to −25 T, not shown) were also included. Figures 3(a)–3(c) show the XRD line profiles of the (130), (060), and (041) reflections measured at 300 K and magnetic fields of 0, 25, and −25 T. Clear shifts in the peak positions of these

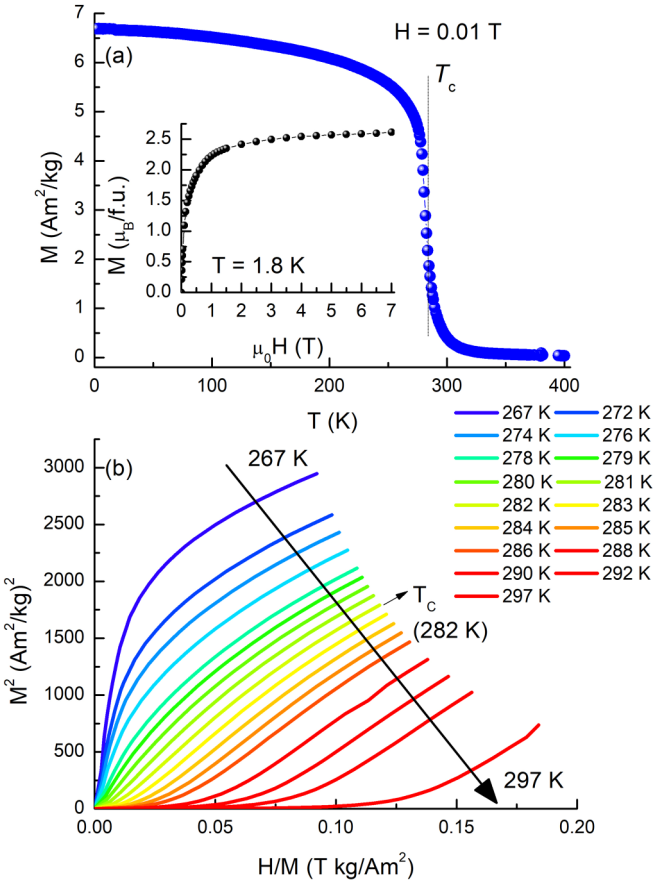

FIG. 2. (a) Temperature dependent zero field cooled magnetization behavior of the sample measured in a field of 10 mT. The FM ordering temperature is indicated by a vertical line. The inset shows the M-vs-H behavior of the sample measured at 1.8 K. (b) Arrott plots measured at several temperatures across T_C ranging 267–297 K. The arrow indicates the direction of increasing temperature.

reflections are observed, while the profile shape remains unchanged. The (130) and (060) reflections shift towards higher 2θ values while the (041) reflection shifts opposite, toward lower 2θ values with increasing magnetic field, indicating that the lattice parameters a and b both decrease while c increases with increasing magnetic field.

To extract a precise field dependence of the orthorhombic lattice parameters, Le Bail fitting of several peaks was carried out [38]. The magnitude and direction of the shift is more pronounced for the (041) reflection as compared to the other two reflections, even though the b axis contracts. This indicates that the applied magnetic field affects the c-axis parameter significantly stronger than the a and b parameters, consistent with DFT results which are discussed in the later section. The refined values of the lattice parameters at 300 K are $a = 2.9292(1)$ Å, $b = 11.0365(4)$ Å, $c = 2.8685(1)$ Å in zero field ($\mu_0 H = 0$ T) and $a = 2.9277(1)$ Å, $b = 11.0300(5)$ Å, $c = 2.8736(1)$ Å at $\mu_0 H = 25$ T, with the number in parentheses the estimated standard deviations derived from the Le Bail fit.

To investigate the effect of the magnetic field on the $AlFe_2B_2$ lattice across the Curie temperature of $T_C = 283$ K, XRD patterns were collected above (290 K) and below (250 K) T_C. Figures 4(a)–4(c) show the field-dependent XRD reflection profiles of the (130), (060), and (041) reflections at 290 K, while Figs. 4(d)–4(f) show the same peak profiles at 250 K. Again, significant angular shifts are observed for the (041) reflection at 290 and 250 K, but with a smaller magnitude at 250 K than at 290 K. Le Bail fits were carried out to obtain the lattice parameters at these temperatures and magnetic fields [38]. For both temperatures, the c axis increases while the a and b axes decrease with increasing magnetic field, as seen in Figs. 5(a) and 5(b). Consequently, the anisotropic strain is positive along the c axis and negative along the a and b axes, as shown in Figs. 6(a)–6(c), with the magnitude of strain maximal along the c axis and minimal along the a axis. The absolute value of the magnetic field is used to plot the data of 250 K for positive ($+ve$) (0 to 25 T) and negative ($-ve$) (0 to −25 T) field cycles in Figs. 5 and 6.

The data show that the change in the c-axis length is more pronounced with temperature and magnetic field than the corresponding changes in the a or b axis. The magnitude of change in the lattice parameters with magnetic field is slightly larger at 290 K than at 300 K and about double that at 250 K, whereas the unit cell volume remains nearly constant at 300 and 290 K while it slightly decreases at 250 K. Therefore, near T_C, the increase in the c axis is compensated by decreases in the a and b axes, but the effect on the c axis is much reduced at 250 K.

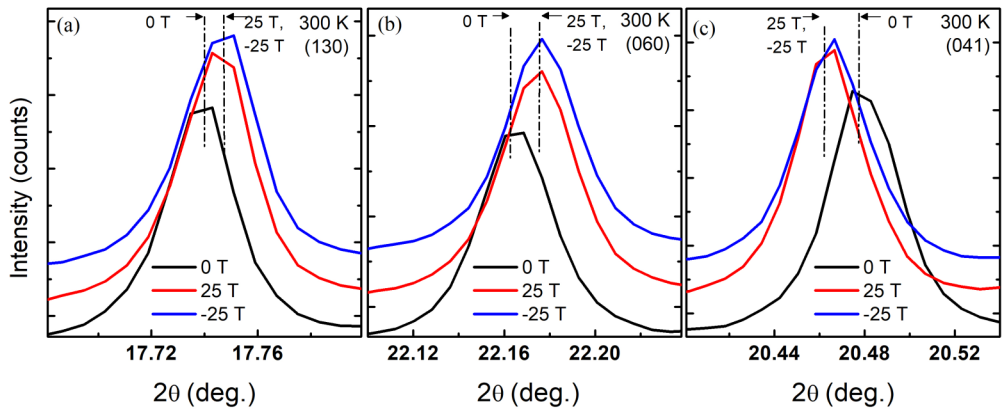

FIG. 3. XRD peak profiles of (a) (130), (b) (060), and (c) (041) reflections recorded at 300 K under 0, 25, and −25 T applied field.

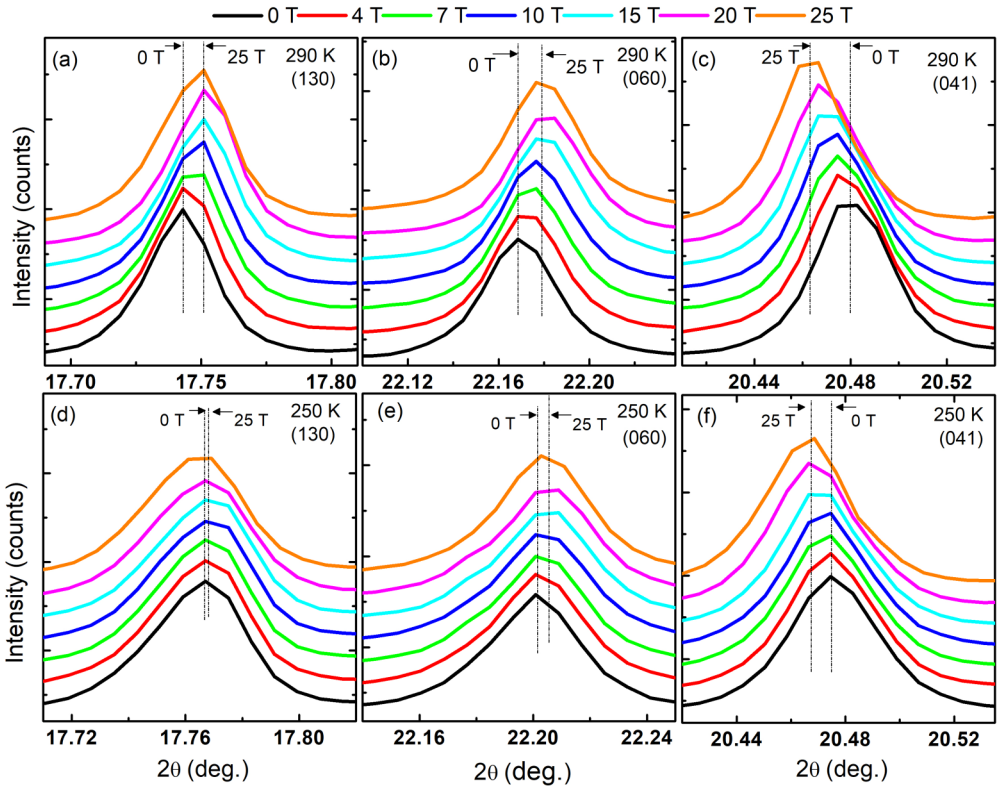

FIG. 4. XRD reflection profiles of (130), (060), and (041) reflections recorded at (a)–(c) 290 K and (d)–(f) 250 K as a function of applied magnetic field. The dashed vertical lines in each panel show the shift in the peak position at 25 T with respect to the signal recorded in the absence of field.

The data in Fig. 5(a) for the temperature of 250 K show a slight asymmetry in the variation of the a and b parameters with positive and negative magnetic field H, whereas the variations in c with magnetic field are symmetric. We would like to point out that it is difficult to estimate the different contributions behind this asymmetry. The raw data do not give a direct measure since there are no reflections exclusive to the a and c axes in the angular range measured. Therefore, full pattern fitting must be used to separate the field dependence of the a, b, and c axes with the magnetic field that has been done in the present work. Another factor that may contribute to the asymmetry in the a and b unit cell parameters is the fact that $AlFe_2B_2$ is in the magnetically ordered state at 250 K, and that the offset reflects the sample history. Consequently, a small hysteretic behavior has been observed for strain values at 250 K between $+ve$ and $-ve$ field cycle. The approximately linear magnetic field induced strain (approximated between 0 and 25 T) gives $\Delta a/a$ of the order of $-1.3594(2)\times10^{-5}\,T^{-1}$ and $-2.3689(1)\times10^{-5}\,T^{-1}$ for $\Delta b/b$, respectively. A similar magnitude for $\Delta c/c$ is found, albeit with opposite sign, $2.7814(2)\times10^{-5}\,T^{-1}$. Furthermore, the magnetic forces on the sample are expected to be larger at 250 K than at 290 and 300 K. Above T_C, i.e., at 290 K, the linear magnetic field induced strain is negative for the a and b axes with values of $-2.3212(1)\times10^{-5}\,T^{-1}$ and $-2.7542(2)\times10^{-5}\,T^{-1}$, respectively, whereas the field induced strain for the c axis is positive and more than doubled to $7.8061(2)\times10^{-5}\,T^{-1}$. It is not possible to estimate the exact volume magnetostriction tensor from our experimental data because the lattice strains are measured at different field orientations with respect to the crystallographic axes. Thus, for any given reflection (hkl), an average signal is measured, which includes contributions from different tensor components. It is therefore expected that the reflections should broaden and shift, to show the averaged strain effect. However, this is not observed within the resolution (full width at half maximum) of the diffractometer. Under the assumption that the magnetic field induced strain is similar for the a and b axes and neglecting off-diagonal terms the tensor can be simplified. Therefore, the values for the magnetic field induced strain represent a first order approximation of the magnetoelastic interactions. As expected, the strain values stay well within the elastic region above and below the magnetic ordering temperature. The volume magnetostriction, which depends on the magnetic field and temperature, has also been plotted and is given in the Supplemental Material (Fig. S3) [39].

The reason for observing a larger change in the *c-axis* parameter at 290 and 300 K as compared to 250 K is as follows: Above T_C, the thermal fluctuations will oppose the effect of the magnetic field on the lattice by counteracting the spin alignment, and below T_C, with ordered spins, the effect of the magnetic field on the lattice will be reduced. Thus, the largest magnetostriction effect is expected near T_C, and decreases on both sides of the transition, due to thermal fluctuations above T_C, and due to spin order below T_C, consistent with Landau theory that predicts the effect to be largest at T_C.

It is interesting to compare the order of magnitude of the effect of temperature and magnetic field on the lattice

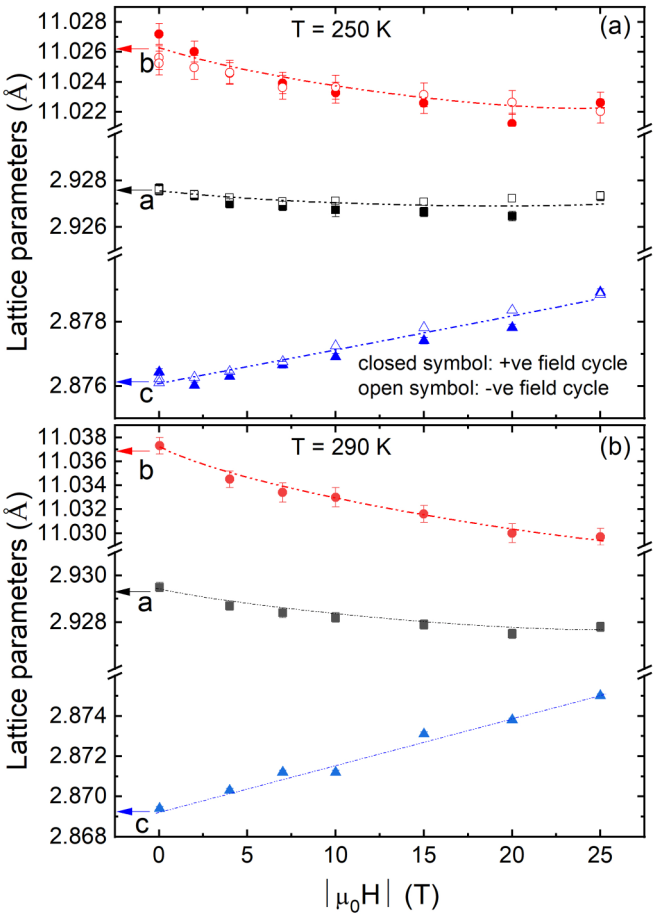

FIG. 5. The field dependence of lattice parameters at (a) 250 K and (b) 290 K. Black squares: *a* axis; red circles: *b* axis; blue triangles: *c* axis. The absolute value of the applied magnetic field is used to plot both the negative $(-ve)$ and positive $(+ve)$ field cycle data of 250 K in (a).

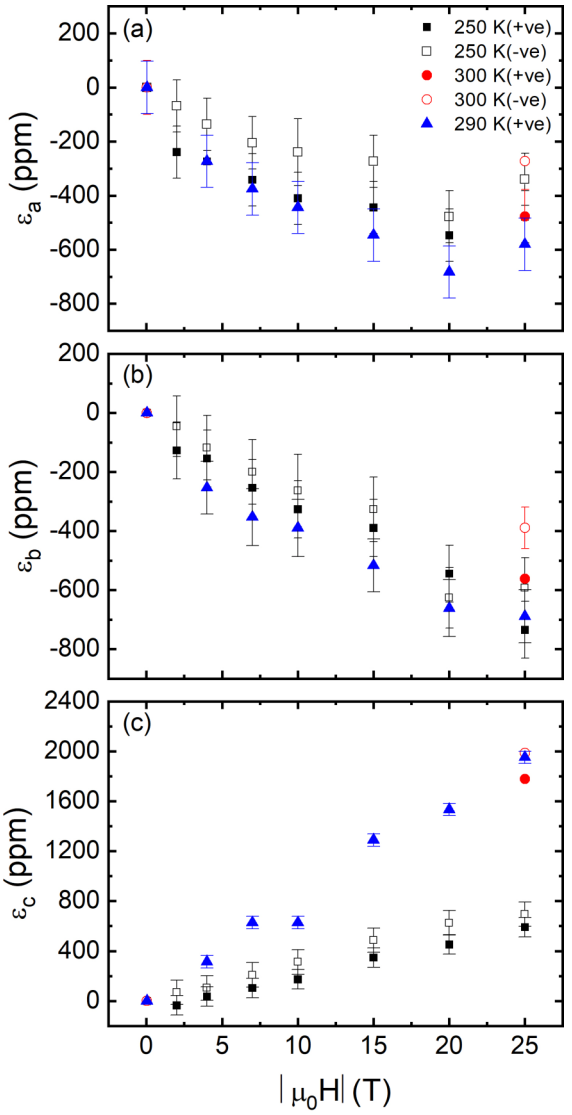

FIG. 6. The anisotropic magnetic field induced strain measured along (a) *a*, (b) *b*, and (c) *c* axis at 250, 290, and 300 K. The strain is positive in the *c* direction while it is negative along the *a* and *b* directions. Absolute magnetic field values are used to plot the field cycle data of 250 and 300 K. The open symbols correspond to the negative field cycle while the closed symbol corresponds to the positive field cycle.

parameters per degree and per tesla in the vicinity of T_C, respectively. These effects are similar, and the details are discussed in the Supplemental Material [39]. To compare the magnetic energy and the strain energy at 25 T, we estimate both in the following way: with the saturation magnetization of 2.06 μ_B/f.u. observed for our sample at 5 T, the magnetic energy $(-MH)$ is of the order of ∼57.5 J/mol at 5 T and ∼287.6 J/mol at 25 T, assuming saturation at 5 T. Using the bulk modulus of 213.42 GPa [41], the density of 5.75 g/cm^3 [23], and the experimentally observed value of strain $(\Delta c/c)$ along the *c* direction at 300 K, the elastic energy is estimated to be about 9.42 J/mol. This indicates that, even at 5 T, the magnetic energy is significantly larger than the elastic energy in $AlFe_2B_2$.

To further evaluate the changes in structural properties under applied magnetic field, we consider the effect of the magnetic field within the framework of a Landau model for the phase transitions [42]. The simplified free energy per unit volume near the transition temperature can be written as [43]

$$f = a(T - T_C)M^2 + \frac{bM^4}{2} - MB + \lambda\varepsilon M^2 + \frac{1}{2}C_{\mathrm{EL}}\varepsilon^2 \quad (1)$$

where *B* is the external magnetic field, *M* the sample magnetization, ε is the strain, and C_{EL} is the elastic tensor. The fourth term $(\lambda\varepsilon M^2)$ is the lowest order magnetoelastic energy coupling the strain and magnetization, and the fifth term $(\frac{1}{2}C_{\mathrm{EL}}\varepsilon^2)$ is the elastic energy contribution to the Gibbs free energy. The magnetostriction is obtained by minimizing Eq. (1) with respect to the strain:

$$\varepsilon = -\frac{\lambda M^2}{C_{\mathrm{EL}}} = NM^2, \quad (2)$$

with $N = -(\lambda/C_{\mathrm{El}})$, a magnetostriction constant. In $AlFe_2B_2$, the magnetostriction is anisotropic, so *N* is a tensor function of both the crystallographic direction and the orientation of the magnetization. If the magnetoelastic energy is small in

comparison to the first three terms in Eq. (1), then M can be estimated by neglecting the last two terms, and the anisotropic magnetostriction terms are obtained from Eq. (2). The field dependence of the magnetization can be evaluated using the Weiss mean field model [44]:

$$M = ng\mu_B S B_S\left(Sg\frac{\mu_B B + \mu_0\gamma\mu_B M}{k_B T}\right) = M_S B_S\left(\frac{\mu_B S g B}{k_B T} + \frac{3S}{S+1}\frac{T_C}{T}\frac{M}{M_s}\right), \quad (3)$$

where B_S is the Brillouin function for the spin S, n is the spin density, g is the gyromagnetic ratio, γ is the molecular field constant, M_s is the saturation magnetization, and $T_C = \mu_0 n g^2 S(S+1)\mu_B^2/3k_B$ is the transition temperature. The change of the magnetostriction with the magnetic field is proportional to $\partial(M^2)/\partial B = 2M(\partial M/\partial B)$. This value diverges at T_C in zero field, and behaves similarly at finite fields. A more accurate model will have to include the effects of the magnetocrystalline anisotropy and the fourth-order coupling terms in magnetization and strain. To establish such a model, however, a detailed study of magnetostriction on a single crystal of $AlFe_2B_2$ is required to determine the magnetoelastic tensor components. The data further suggest that the magnetostriction in this material has higher order terms. Figure S3 also shows that the variation in lattice parameters with magnetic field is temperature dependent, with the largest effect near T_C. For any linear combinations of magnetostrictive strains, the result will be also a linear function of M^2. Since M^2 is increasing monotonically with the field, the linear combination of strains must also be a monotonic function, contrary to what is observed (Fig. S3). Within the linear approximation, the magnetoelastic terms λ can be estimated using our magnetostriction data and the Brillouin function for $S = 1/2$. Using an approximate value of 1.2 μ_B/Fe atom, $S = 1/2$ is a reasonable approximation. At T_C and in a magnetic field of 25 T, the square of the normalized magnetization, M^2/M_S^2, should be about 0.25 according to Eq. (3). Our experimental data show that the relative elongation for the c axis is about 0.002. The magnetostriction constant N from Eq. (2) calculates to about $3.7\times10^{-14}\,\mathrm{m^2/A^2}$ for a saturation magnetization of 1.2 μ_B per Fe ion. For simplicity, the same value can be used for the elastic constant as was used for the bulk modulus. The magnetoelastic energy term λ is then estimated to be about $-0.0074\,\frac{J}{\mathrm{A^2\,m}}$ for the c axis, whereas values for the other axes are about half and of opposite sign, e.g., $0.0037\,\frac{J}{\mathrm{A^2\,m}}$. The analysis using Landau theory is indeed limited due to the fact that a powder sample is used, and therefore, the magnetoelastic response is averaged over all possible orientations.

The linear behavior of the magnetic field induced strain is contrasted by the Landau theory derived equation that relates the strain to the square of the magnetization. In $AlFe_2B_2$, the relationship between magnetization and applied field needs to be considered. Above T_C, the $M(H)$ function can be approximated by a square root relationship $M \propto H^{1/2}$, resulting in an almost linear behavior of the strain with applied magnetic field. Below T_C, the magnetization increases rapidly for small fields, and for an external field of $\mu_0 H > 1$ T at 267 K, a simple power law fit gives $M \propto H^{1/8}$. It is therefore expected that below T_C, the strain versus external magnetic field relationship will not be linear. While this is observed for the a and b axes (as evident in Fig. 5), the c axis increases almost linearly up to 25 T. However, the magnitude of the c-axis strain is clearly reduced at 250 K as compared to 290 K.

TABLE I. Results of geometry optimization for $AlFe_2B_2$ in the nonpolarized and spin-polarized (ferromagnetic) models.

Parameter	Nonpolarized	Spin-polarized	Relative change
a (Å)	2.9297	2.9153	–0.49%
b (Å)	11.3485	11.0247	–2.94%
c (Å)	2.69676	2.8487	5.33%

Landau theory predicts a jump in the thermal expansion coefficient at T_C, which is observed in the data presented by Oye *et al.* [32]. Landau theory further allows linking this jump at T_C to the magnetoelastic coefficient. In zero magnetic field, the Fe moments are aligned along the a axis, thus the thermal expansion changes along the b and c axes are similar to our XRD measurements where we measure the interplanar distance change perpendicular to an external field. The values of $(4.2\pm0.1)\times10^{-5}\,\mathrm{K^{-1}}$ (b axis) and $(-1.2\pm0.1)\times10^{-4}\ \mathrm{K^{-1}}$ (c axis) are found using the temperature dependent XRD data at zero field. If the jump in the thermal expansion coefficient is due to the appearance of the spontaneous magnetic moment below T_C, it can be estimated according to Eq. (2). The magnetic moment below T_C is estimated by using the Taylor expansion of the Brillouin function for $S = 1/2$ near T_C at zero magnetic field: $M^2 \approx 3M_s^2(1-T/T_C)$. Using this temperature dependence for the magnetization and the magnetoelastic constant λ, the jump in the thermal expansion is about $-8\times10^{-5}\ \mathrm{K^{-1}}$, close to the observed values as mentioned above. The sign of the effect at zero field is in agreement with our experimental results: the c axis expands while the b axis contracts if the magnetization is perpendicular to them.

As expected for a magnetocaloric material, the response of the lattice to an external magnetic field is, to first order, similar to lowering the temperature of the system, Comparable magnitudes in the effects on the lattice parameters are observed, and the effect on the c axis is largest at T_C, consistent with Landau theory, and is reduced to about a third at 250 K.

To understand the influence of ferromagnetic order on the lattice parameters of $AlFe_2B_2$, we also performed DFT calculations on the non-spin-polarized and spin-polarized (ferromagnetic) models, starting with the experimentally determined structure [22]. Details of the calculations are given in the Supplemental Material [39,40,45–48]. The unit cell parameters obtained after geometry optimization are listed in Table I. As can be seen from these results, the spin polarization has a minor effect on the a axis, which contracts only slightly, while a somewhat larger contraction is observed for the b axis. The c axis, in contrast, elongates by more than 5%, moving the iron atoms further apart. The results of our calculations are in good qualitative agreement with the changes in the unit cell parameters calculated by Ke *et al.* [30], and they agree with the experimental observation of small contractions along the a and b axes and a larger expansion along the c axis upon application of high magnetic field near T_C (Fig. 5).

IV. CONCLUSIONS

$AlFe_2B_2$ exhibits anisotropic magnetostriction in an applied DC magnetic field up to 25 T. The unit cell parameter c increases while the a and b axes decrease with increasing magnetic field, with the largest effect for the elongation of the c axis (see Fig. 5) in the vicinity of T_C, consistent with DFT calculations. Close to T_C, at 300 and 290 K, the magnitude of the magnetostriction is larger than at 250 K. Furthermore, the fourth order magnetoelastic energy terms in magnetization should be comparable to the quadratic terms. A Landau theory model including quartic terms gives qualitative good agreement with the observed behavior of $AlFe_2B_2$ in high magnetic fields. The model correctly predicts that the magnetostrictive effects are largest in the vicinity of T_C and drop off for higher and lower temperatures. While not all tensor components of the magnetoelastic tensor can be determined from powder diffraction measurements in high magnetic fields, the x-ray diffractometer for the Florida split coil 25 T magnet at the NHMFL has been instrumental in assessing the model for magnetostriction based on Landau theory. Additionally, due to the mostly linear effect of the changes in the unit cell axes with applied field, a simple empirical relationship relating strain to the external magnetic field can be given, with values for the a axis as -2.29×10^{-5} T^{-1}, for the b axis as -2.60×10^{-5} T^{-1}, and for the c axis as 7.81×10^{-5} T^{-1} for absolute magnitudes of the magnetic field (see also the Supplemental Material [39]). While the magnetostriction along the a and b axes are almost independent of temperature, the magnetostriction is reduced at lower temperature along the c axis, resulting in an overall negative volume magnetostriction at 250 K. The results of DFT calculations support the observed anisotropic changes in the lattice parameters of $AlFe_2B_2$ caused by ferromagnetic alignment of Fe moments.

ACKNOWLEDGMENTS

This work was supported by the National Science Foundation under Award No. DMR-1625780. Part of the work was carried out at the National High Magnetic Field Laboratory, which is supported by the National Science Foundation under Cooperative Agreement No. DMR-1644779 and the State of Florida.

[1] N. A. Spaldin and R. Ramesh, Advances in magnetoelectric multiferroics, Nat. Mater. **18**, 203 (2019).

[2] C. De, N. V. Ter-Oganessian, and A. Sundaresan, Spin-driven ferroelectricity and large magnetoelectric effect in monoclinic $MnSb_2S_4$, Phys. Rev. B **98**, 174430 (2018).

[3] H. E. Karaca, I. Karaman, B. Basaran, Y. Ren, Y. I. Chumlyakov, and H. J. Maier, Magnetic field-induced phase transformation in NiMnCoIn magnetic shape-memory alloys—a new actuation mechanism with large work output, Adv. Funct. Mater. **19**, 983 (2009).

[4] J. Liu, Y. Gong, G. Xu, G. Peng, I. A. Shah, N. Hassan, and F. Xu, Realization of magnetostructural coupling by modifying structural transitions in MnNiSi-CoNiGe system with a wide curie-temperature window, Sci. Rep. **6**, 23386 (2016).

[5] K. A. Gschneidner Jr., V. K. Pecharsky, and A. O. Tsokol, Recent developments in magnetocaloric materials, Rep. Prog. Phys. **68**, 1479 (2005).

[6] O. Gutfleisch, M. A. Willard, E. Brück, C. H. Chen, S. G. Sankar, and J. P. Liu, Magnetic materials and devices for the 21st century: Stronger, lighter, and more energy efficient, Adv. Mater. **23**, 821 (2011).

[7] R. Kainuma, Y. Imano, W. Ito, Y. Sutou, H. Morito, S. Okamoto, O. Kitakami, K. Oikawa, A. Fujita, T. Kanomata, and K. Ishida, Magnetic-Field-Induced shape recovery by reverse phase transformation, Nature (London) **439**, 957 (2006).

[8] V. K. Pecharsky and K. A. Gschneidner, Jr., Giant Magnetocaloric Effect in $Gd_5Si_2Ge_2$, Phys. Rev. Lett. **78**, 4494 (1997).

[9] J. Liu, T. Gottschall, K. P. Skokov, J. D. Moore, and O. Gutfleisch, Giant magnetocaloric effect driven by structural transitions, Nat. Mater. **11**, 620 (2012).

[10] M. Chmielus, X. X. Zhang, C. Witherspoon, D. C. Dunand, and P. Müllner, Giant magnetic-field-induced strains in polycrystalline Ni–Mn–Ga foams, Nat. Mater. **8**, 863 (2009).

[11] Y. H. Matsuda, A. Shimizu, A. Ikeda, T. Nomura, T. Yajima, T. Inami, K. Takahashi, and T. C. Kobayashi, High magnetic field x-ray diffraction study of the alph-phase of solid oxygen: absence of giant magnetostriction, Phys. Rev. B **100**, 214105 (2019).

[12] S. Sharma, A. Shahee, P. Yadav, I. Da Silva, and N. P. Lalla, In-field x-ray and neutron diffraction studies of re-entrant charge-ordering and field induced metastability in $La_{0.175}Pr_{0.45}Ca_{0.375}MnO_{3-\delta}$, J. Appl. Phys. **122**, 175902 (2017).

[13] V. K. Sharma, M. K. Chattopadhyay, K. H. B. Shaeb, A. Chouhan, and S. B. Roy, Large magnetoresistance in $Ni_{50}Mn_{34}In_{16}$ Alloy, Appl. Phys. Lett. **89**, 222509 (2006).

[14] X. Tan, P. Chai, C. M. Thompson, and M. Shatruk, Magnetocaloric effect in $AlFe_2B_2$: Toward magnetic refrigerants from earth-abundant elements, J. Am. Chem. Soc. **135**, 9553 (2013).

[15] B. T. Lejeune, D. L. Schlagel, B. A. Jensen, T. A. Lograsso, M. J. Kramer, and L. H. Lewis, Effects of Al and Fe solubility on the magnetofunctional properties of $AlFe_2B_2$, Phys. Rev. Mater. **3**, 094411 (2019).

[16] R. Barua, B. T. Lejeune, L. Ke, G. Hadjipanayis, E. M. Levin, R. W. McCallum, M. J. Kramer, and L. H. Lewis, Anisotropic magnetocaloric response in $AlFe_2B_2$, J. Alloys Compd. **745**, 505 (2018).

[17] Z. Zhang, G. Yao, L. Zhang, P. Jia, X. Fu, W. Cui, and Q. Wang, Magnetic phase transition and room-temperature magnetocaloric effects in (Al, M)Fe_2B_2 (M = Si, Ga) compounds, J. Magn. Magn. Mater. **484**, 154 (2019).

[18] S. C. Ma, D. Hou, Y. Y. Gong, L. Y. Wang, Y. L. Huang, Z. C. Zhong, D. H. Wang, and Y. W. Du, Giant Magnetocaloric and magnetoresistance effects in ferrimagnetic $Mn_{1.9}Co_{0.1}Sb$ Alloy, Appl. Phys. Lett. **104**, 022410 (2014).

[19] V. K. Sharma, M. A. Manekar, H. Srivastava, and S. B. Roy, Giant magnetocaloric effect near room temperature in the off-stoichiometric Mn–Co–Ge Alloy, J. Phys. D: Appl. Phys. **49**, 50LT01 (2016).

[20] M. Das, S. Roy, N. Khan, and P. Mandal, Giant magnetocaloric effect in an exchange-frustrated $GdCrTiO_5$ antiferromagnet, Phys. Rev. B **98**, 104420 (2018).

[21] P. K. Das, A. Bhattacharyya, R. Kulkarni, S. K. Dhar, and A. Thamizhavel, Anisotropic magnetic properties and giant magnetocaloric effect of single-crystal PrSi, Phys. Rev. B **89**, 134418 (2014).

[22] W. Jeitschko, The crystal structure of Fe_2AlB_2, Acta Cryst. B **25**, 163 (1969).

[23] T. N. Lamichhane, L. Xiang, Q. Lin, T. Pandey, D. S. Parker, T.-H. Kim, L. Zhou, M. J. Kramer, S. L. Bud'ko, and P. C. Canfield, Magnetic properties of single crystalline itinerant ferromagnet $AlFe_2B_2$, Phys. Rev. Mater. **2**, 084408 (2018).

[24] M. ElMassalami, D. da, S. Oliveira, and H. Takeya, On the ferromagnetism of $AlFe_2B_2$, J. Magn. Magn. Mater. **323**, 2133 (2011).

[25] L. H. Lewis, R. Barua, and B. Lejeune, Developing magneto-functionality: coupled structural and magnetic phase transition in $AlFe_2B_2$, J. Alloys Compd. **650**, 482 (2015).

[26] E. M. Levin, B. A. Jensen, R. Barua, B. Lejeune, A. Howard, R. W. McCallum, M. J. Kramer, and L. H. Lewis, Effects of Al content and annealing on the phases formation, lattice parameters, and magnetization $Al_xFe_2B_2$ ($X = 1.0, 1.1, 1.2$) alloys, Phys. Rev. Mater. **2**, 034403 (2018).

[27] J. W. Lee, M. S. Song, B. K. Cho, and C. Nam, Magnetic properties of pure $AlFe_2B_2$ formed through annealing followed by acid-treatment, Curr. Appl. Phys. **19**, 933 (2019).

[28] T. Ali, M. N. Khan, E. Ahmed, and A. Ali, Phase analysis of $AlFe_2B_2$ by synchrotron x-ray diffraction, magnetic and Mössbauer studies, Prog. Nat. Sci. Mater. Int. **27**, 251 (2017).

[29] J. Cedervall, M. S. Andersson, T. Sarkar, E. K. Delczeg-Czirjak, L. Bergqvist, T. C. Hansen, P. Beran, P. Nordblad, and M. Sahlberg, Magnetic structure of the magnetocaloric compound $AlFe_2B_2$, J. Alloys Compd. **664**, 784 (2016).

[30] L. Ke, B. N. Harmon, and M. J. Kramer, Electronic structure and magnetic properties in T_2AlB_2 (T = Fe, Mn, Cr, Co, and Ni) and their alloys, Phys. Rev. B **95**, 104427 (2017).

[31] B. T. Lejeune, B. A. Jensen, R. Barua, E. Stonkevitch, R. W. McCallum, M. J. Kramer, and L. H. Lewis, Lattice-driven magnetic transitions in Al(Fe,T)2×2 compounds, J. Magn. Magn. Mater. **481**, 262 (2019).

[32] Y. M. Oey, J. D. Bocarsly, D. Mann, E. E. Levin, M. Shatruk, and R. Seshadri, Structural changes upon magnetic ordering in magnetocaloric $AlFe_2B_2$, Appl. Phys. Lett. **116**, 212403 (2020).

[33] S. Wang, A. E. Kovalev, A. V Suslov, and T. Siegrist, A facility for x-ray diffraction in magnetic fields up to 25 T and temperatures between 15 and 295 K, Rev. Sci. Instrum. **86**, 123902 (2015).

[34] *AXO Dresden GmbH - Applied X-ray Optics and High Precision Deposition*, Gasanstaltstr, 8b (Weißes Haus/White House) Dresden, Germany.

[35] J. Filik, A. W. Ashton, P. C. Y. Chang, P. A. Chater, S. J. Day, M. Drakopoulos, M. W. Gerring, M. L. Hart, O. V Magdysyuk, S. Michalik, A. Smith, C. C. Tang, N. J. Terrill, M. T. Wharmby, and H. Wilhelm, Processing two-dimensional x-ray diffraction and small-angle scattering data in *DAWN 2*, J. Appl. Cryst. **50**, 959 (2017).

[36] D. R. Black, D. Windover, A. Henins, J. Filliben, and J. P. Cline, Certification of standard reference material 660B, Powder Diffr. **26**, 155 (2011).

[37] V. Petříček, M. Dušek, and L. Palatinus, Crystallographic computing system JANA2006: General features, Z. Kristallogr. **229**, 345 (2014).

[38] A. Le Bail, H. Duroy, and J. L. Fourquet, Ab-Initio structure determination of $LiSbWO_6$ by x-ray powder diffraction, Mater. Res. Bull. **23**, 447 (1988).

[39] See Supplemental Material at http://link.aps.org/supplemental/10.1103/PhysRevMaterials.5.064409 for the calibration of the detector, magnetostriction data, and DFT calculations.

[40] G. Kresse and J. Furthmüller, Efficient iterative schemes for ab initio total-energy calculations using a plane-wave basis set, Phys. Rev. B **54**, 11169 (1996).

[41] R. Wang, X. Tao, Y. Ouyang, H. Chen, and Q. Peng, Suggest a new approach to fabricate $AlFe_2B_2$, Comput. Mater. Sci. **171**, 109239 (2020).

[42] L. D. Landau and E. M. Lifshitz, Phase transition of the second kind and critical phenomena, in *Statistical Physics*, 3rd ed. (Butterworth-Heinemann, Oxford, 1980), pp. 446–516.

[43] M. E. McHenry and D. E. Laughlin, Theory of magnetic phase transitions, in *Characterization of Materials*, edited by E. N. Kaufmann (John Wiley & Sons, 2012).

[44] J. Patterson and B. Bailey, in *Solid State Physics* (Springer, Berlin, Heidelberg, 2010), pp. 355–462.

[45] G. Kresse and J. Hafner, Ab initio molecular dynamics for liquid metals, Phys. Rev. B **47**, 558 (1993).

[46] G. Kresse and J. Hafner, Ab initio molecular-dynamics simulation of the liquid-metal–amorphous-semiconductor transition in germanium, Phys. Rev. B **49**, 14251 (1994).

[47] G. Kresse and J. Furthmüller, Efficiency of ab-initio total energy calculations for metals and semiconductors using a plane-wave basis set, Comput. Mater. Sci. **6**, 15 (1996).

[48] J. P. Perdew, K. Burke, and M. Ernzerhof, Generalized Gradient Approximation Made Simple, Phys. Rev. Lett. **77**, 3865 (1996); **78**, 1396(E) (1997).